Sixth International Symposium on Marine Propulsors
smp'19, Rome, Italy, May 2019

Instability identification within ship propeller wakes

Shakeel Ahmed*, Paul Croaker, and Con Doolan

School of Mechanical and Manufacturing Engineering, UNSW, Sydney, Australia

ABSTRACT

Large eddy simulations are performed on the INSEAN E779a benchmark ship propeller. The propeller is a four bladed constant pitch, lightly skewed model with a diameter of 227 mm and sheds strong tip vortices thus making it suitable for wake instability analysis. The flow past the propeller is at a Reynolds number of 2 x 10^6 based on the reference tip velocity of 17.85 m/s and reference length equivalent to the propeller radius.

A high-fidelity mesh of approximately 24 million cells is used to resolve the propeller flow characteristics. Simulations describe adequately the ship propeller wake vortical structures from their evolution in the near wake to their breakdown in the far wake. Simulation results compare favorably with available experimental data in the literature thus validating the applicability of the current work.

Wake instabilities are shown to commence in the transition region, thus making this part of the wake highly important to understanding the mechanisms of propeller wake breakdown. A new instability mechanism involving the mutual interaction of helical vortex sheets is observed in the transition region. The influence and interaction of the helical vortex sheets with the tip and hub vortices is highlighted with particular attention given to their role in the onset and growth of short and long wave wake instabilities. The detail of how the mutual interaction between tip vortex filaments occurs is also presented. As a result of the simulations and resulting analysis, instability instigating mechanisms in the propeller wake are identified and appropriately correlated.

Keywords

LES, Ship propeller wake, Tip vortex, Helical vortex sheets.

1 INTRODUCTION

The propeller wake is composed of vortical structures, shed from the blade trailing edges that roll up due to changing pressures across the blade surfaces. Among these vortical structures formed, two are filament type having set thicknesses. The one formed at the tip of each blade is called tip vortex and the other combined at the root sections of the blade is called the hub vortex. Also shed are sheets of vorticity called helical vortex sheets from the whole trailing edge of each blade due to non-constant circulation over the blade surfaces. Overall the propeller wake can be classified into three regions based on distinct flow phenomenon:

i. Near wake – Wake evolves and rolls up and then undergoes the slipstream contraction
ii. Transition wake – Wake vortical structures slowly destabilize
iii. Far wake: Wake breaks down totally.

How the wake breakdown occurs in the far wake is yet to be understood completely. Fundamental research on the stability of a single helical vortex filament with respect to spatial perturbations was performed by Widnall (1972). She identified three instability modes, namely short waves occurring inside filament cores, long waves displacing the whole filament and mutual interaction mode among adjacent filaments. Gupta & Loewy (2004) and Okulov & Sørensen (2007) extended the theoretical analysis to systems of helices, including the hub vortex in the later study.

The instability modes as mentioned above and predicted by the theoretical approaches have been observed generally in numerical and experimental studies. However, Felli et al (2011) noted the ineffectiveness of the above models for predicting stability boundaries of ship propeller wakes in a land mark experimental study. The study concluded many earlier experimental works on ship propeller wakes predominantly carried out at INSEAN. Felli et al (2011) determined that the mutual-inductance mode among adjacent helical filaments drives the transition to an unstable wake.

Recently, however, using large eddy simulations (LES), Mahesh & Kumar (2017) simulated the propeller wake from a weakly loaded propeller. They presented a new assessment that mutual-interaction between the tip vortex

*Corresponding author: Shakeel Ahmed

E-mail address: shakeel.ahmed@unsw.edu.au.

and the smaller vortices in the helical vortex sheets play the major role in wake instabilities for propellers with weak tip vortices.

Thus a concluding consensus regarding mechanisms leading to ship propeller wake instabilities is yet to be reached. This warrants further studies so as to have a full understanding of the wake behaviour behind ship propellers. The research reported here is an initial part of current work being carried out in this regard.

In the present work, hydrodynamic analyses are performed using LES to gain a thorough understanding of propeller wake flow physics. The analyses presented are at a relatively higher advance coefficient (J = 0.75), as the wake is of sufficient length to study and identify as many mechanisms as possible leading to ship propeller wake breakdowns. The objectives are (a) to describe ship propeller wake geometry appropriately using LES for a benchmark ship propeller shedding stronger tip vortices and (b) gain insight into the non-linear propeller wake evolution and breakdown mechanisms.

2 NUMERICAL FLOW ANALYSES

2.1 Test Case

The test case is a benchmark four bladed ship propeller INSEAN E779A of model scale dimensions (Figure 1). The propeller has constant pitch, and is lightly skewed with a model scale diameter, D of 0.227 m. The primary dimensions and operating parameters are as given in Table 1. The loading condition defined by advance coefficient of J = 0.75 is calculated from:

$$J = \frac{U_\infty}{nD} \tag{1}$$

Where U_∞ represents the free stream inflow velocity while n is the propeller rotation rate.

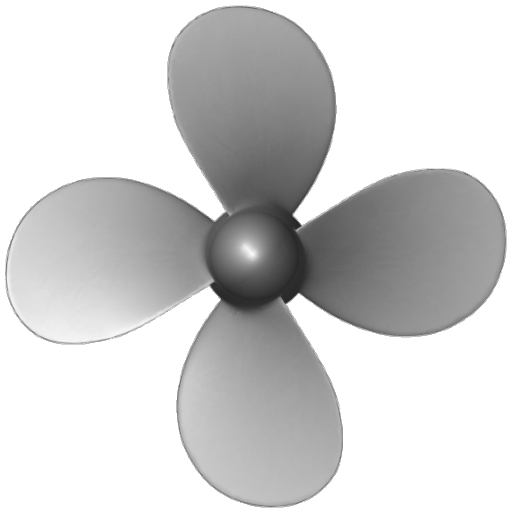

Figure 1: INSEAN E779A propeller geometry

Table 1: Primary operating parameters – INSEAN E779A

Description	Dimensions
Propeller Diameter, *D*	0.227 m
Reference chord, *B*	0.087 m
Pitch ratio, *P/D*	1.1
Rake	$4^o35'$ (forward)
Rotaional Speed, *n*	1500 rpm
Reynold Number, *Re*	2×10^6

2.2 Numerical Theory

To intrinsically account for all the propeller hydrodynamics effects, full three-dimensional, unsteady, incompressible, and viscous turbulent flow realized by solution of the continuity and Navier Stokes equations using direct numerical simulation (DNS), is required.

In DNS there is no turbulence modelling and all the turbulence scales are resolved. DNS however, requires extremely fine meshing and is thus computationally not feasible for ship propeller research at present. Large eddy simulations on the other hand resolve turbulent fluctuations in the inertial subrange of scales while modelling the smaller scales. Therefore, LES is a promising technique for propeller wake studies as the interactions between the resolved scales is expected to dominate the generation, evolution and breakdown of propeller wake structures.

In present work large eddy simulation modelling techniques as available in ANSYS FLUENT (2016) are employed. Here the flow field division is accomplished by employing a spatial filtering function based on the finite volume method. This separates the turbulent flow into larger resolved eddies (filtered field defined by variable $\bar{\Phi}$), and smaller modelled eddies (sub-grid scale field defined by Φ'). The corresponding filtered variable $\bar{\Phi}$ is calculated from volume V of the mesh cell as:

$$\bar{\Phi}(x) = \frac{1}{\mathrm{V}} \int_v \Phi(x') dx' \quad , \quad x' \in v \tag{2}$$

To fully resolve relevant turbulent eddies the filtered continuity (3) and Navier Stokes equations (4) for LES are then derived as:

$$\frac{\partial}{\partial x_i}(\rho \overline{u}_i) = 0 \tag{3}$$

$$\frac{\partial}{\partial t}(\rho \overline{u}_i) + \frac{\partial}{\partial x_j}(\rho \overline{u}_i \overline{u}_j) = -\frac{\partial \overline{p}}{\partial x_i} + \frac{\partial}{\partial x_j}\left[\mu\left(\frac{\partial \overline{u}_i}{\partial x_j} + \frac{\partial \overline{u}_j}{\partial x_i} - \frac{2}{3}\delta_{ij}\frac{\partial \overline{u}_l}{\partial x_l}\right)\right] - \frac{\partial}{\partial x_j}\left(\rho \overline{u_i u_j} - \rho \overline{u}_i \overline{u}_j\right) \tag{4}$$

Where u_i and u_j are the instantaneous velocities, p the pressure, ρ the fluid density, μ the dynamic viscosity and δ_{ij} the Kronecker delta. The essential flow statistics contained in the larger eddies are thus resolved and the LES convergence towards the exact solution can be increased by refining the mesh size (depending on

available resources). Normally, the effects of the sub-grid residual structures are not entirely discarded and as such are represented by an additional term in the filtered Navier Stokes equation (4). These sub-grid-scales stresses τ_{ij} are modelled using the Boussinesq hypothesis:

$$\tau_{ij} = \rho\overline{u_i u_j} - \rho\overline{u}_i\overline{u}_j = \mu_t\left(\frac{\partial\overline{u}_i}{\partial x_j} + \frac{\partial\overline{u}_j}{\partial x_i}\right) - \frac{1}{3}\delta_{ij}\tau_{kk} \qquad (5)$$

The residual stresses represented by τ_{kk} are isotropic, thus requiring no further modelling and are added to filtered static pressure term. This leaves turbulent viscosity μ_t, as the only parameter requiring modelling in above equation, which is accomplished through an appropriate sub-grid scale model.

In case the mesh satisfies the guidelines for wall resolved LES: Δx^+ = 100, wall y^+ = 1 and Δz^+ = 30 (Davidson 2009); Smagorinsky-Lilly model is typically preferred to model the turbulent viscosity μ_t. This is possible for simplified cases where a very fine mesh for complete resolution of eddies in the near wall-region can easily be generated. However, such a fine mesh increases the overall grid size substantially for wall-bounded flows in general and for propeller wake in particular due to a fine, isotropic mesh required for a considerable distance downstream of the propeller to accurately resolve the wake. Shur et al. (2008) solved this problem by proposing a modified Smagorinsky model along-with a mixing length model. This methodology triggers RANS only in the inner part of the logarithmic layer while the remaining boundary layer is resolved. The use of Shur et al. (2008) methodology for sub-grid length scales is viable not only for wall-modelled LES cases but is also advantageous for the wall-resolved large eddy simulations (Shur et al. 2008). For that reason, and to keep the total number of cells to a practicable total, the Shur et al. (2008) methodology is used in the current work for sub-grid scale modelling.

2.2 Numerical Setup

Ansys DesignModeler is used to model the propeller geometry (Figure 1) and the computational domain (Figure 2). The computational domain is based on similar size and setup as those in experiments (Felli et al 2011) to avoid blockage effects (Stella et al 2000). This also ensures an appropriate comparison with experimental wake vortical structures and other data available in literature for this benchmark ship propeller INSEAN E779A.

The domain diameter is approximately 3 propeller diameters while the length of the computational domain is approximately 12 propeller diameters. As for the boundary conditions (Figure 2); at the inlet a velocity of 4.25 meter/second is specified based on the free stream velocity for this specific advance coefficient while atmospheric pressure is specified at outlet. No-slip rotating wall boundary condition is applied on the propeller surfaces with a rotation rate of 1500 rpm. The

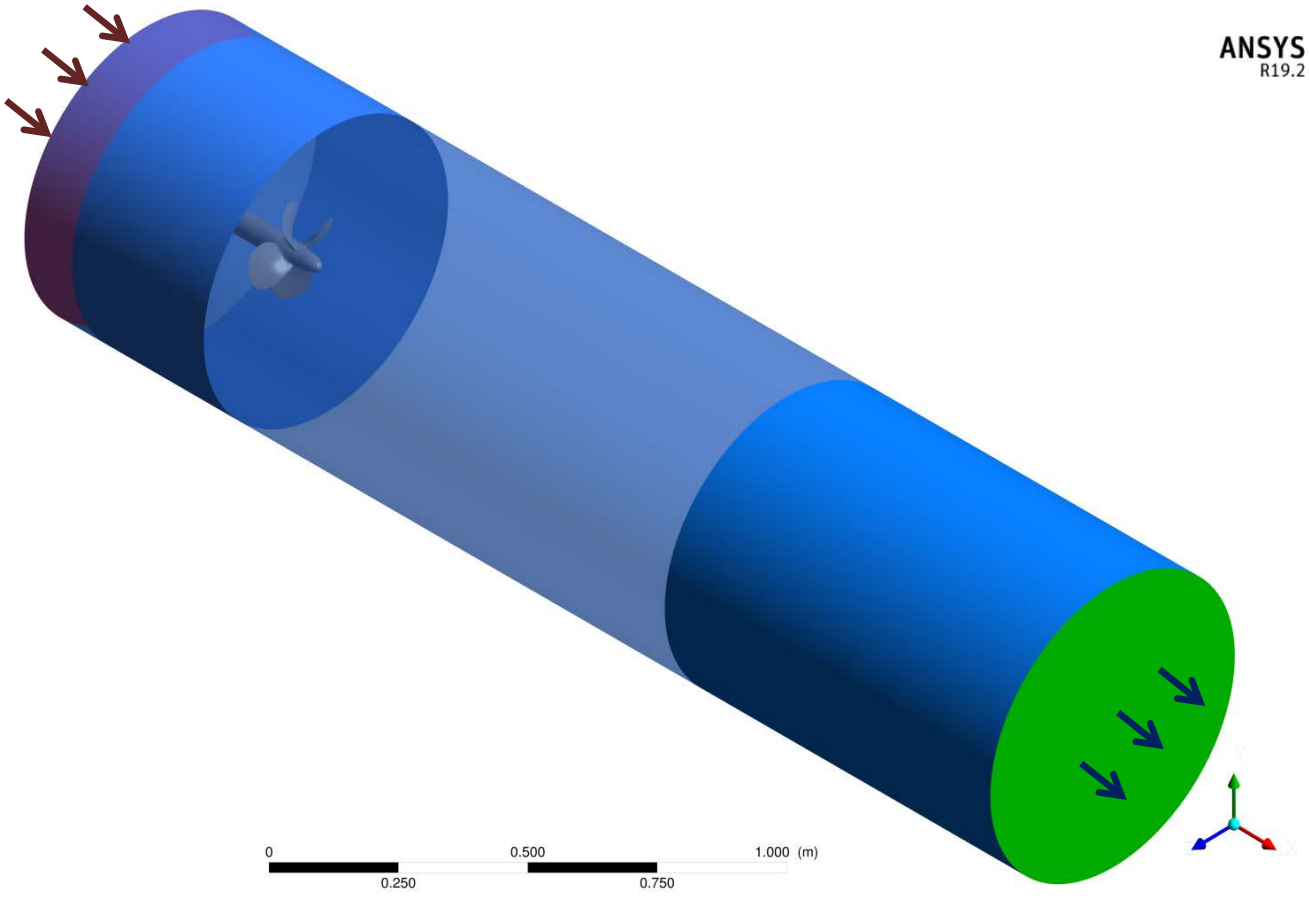

Figure 2: Computational domain and boundary Conditions

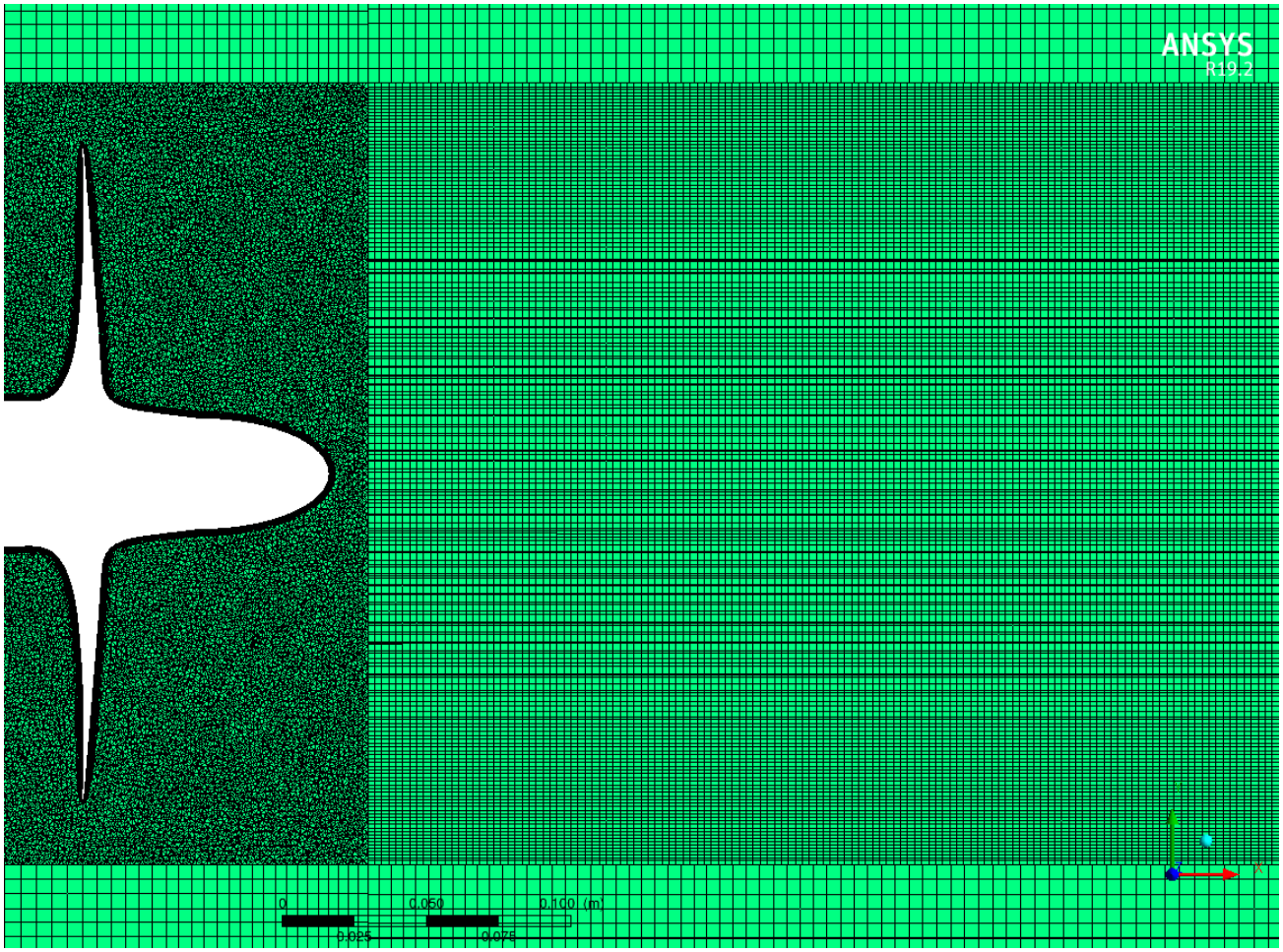

Figure 3: Mesh on the mid-longitudinal plane *XY*

outer walls are assigned zero shear boundary condition.

Ansys Workbench Mesh is employed to create, generate and export mesh to the FLUENT solver. The mesh generated is a hybrid grid composed of tetrahedral, prisms and pyramids. The propeller surfaces are meshed with triangular surfaces to better capture the curved blade faces and also to reduce meshing time and effort. From the tri-surfaces fine boundary layer prisms are extruded to capture the boundary layer effects and to have wall $y^+ \sim 1$. In this regard to resolve maximum eddies in the wall-boundary layer region, the current mesh on the propeller blades has a streamwise resolution of $\Delta x^+ = 250$, wall normal resolution of $y^+ = 1$, and spanwise resolution of $\Delta z^+ = 250$. After the prism boundary layer the area surrounding the propeller blades is meshed with a fine distribution of tetrahedral cells to capture the wake evolution correctly. From that point forward a cylinder of fine isotropic cells extends approximately six propeller diameters encompassing the entire propeller wake downstream. This ensures that the coherent vortical structures of interest are adequately resolved. The overall mesh size is about 24 million cells. A preview of the generated mesh on the central-longitudinal plane is shown in Figure 3.

Solution of the generated mesh has been carried out using the ANSYS FLUENT flow solver. Unsteady Reynolds-averaged Navier–Stokes equations (URANS) are employed to generate an initial flow solution. The flow field from the URANS simulations is then used to initialize the computationally expensive LES. Shear stress transport (SST) k-ω model is used to model turbulence for URANS. While Shur et al. (2008) based LES (WMLES S-Omega) is employed for the wake flow analyses. For solution discretization initially first order schemes are employed and after stability of the solution is achieve, the schemes are switched to higher order upwind schemes. To simulate the dynamic response of the propeller; the propeller and its surrounding mesh is set to physically rotate with the remaining portion of the domain fixed in space.

2.3 Results

The propeller performance characteristics, also known as the global characteristics, are represented by thrust and torque coefficients. The thrust (K_t) and toque (K_q) coefficients are calculated from the forces T and moments Q acting on the propeller blades & hydrodynamic flow characteristics and are given as:

$$K_t = \frac{T}{\rho n^2 D^4} \tag{6}$$

$$K_q = \frac{Q}{\rho n^2 D^5} \quad (7)$$

These global characteristics are predicted well by the current LES analyses when compared with experiments (Salvatore et al 2006) as shown in the Table 2 below.

Table 2: INSEAN E779A – Performance characteristics

Parameter	*J*	LES	EXP	Error
Thrust Coefficient	0.75	0.218	0.222	2.0%
Torque Coefficient	0.75	0.041	0.040	2.6%

The propeller wake vortical structures composed of tip and hub vortical filaments are visualized by using Q-criterion. Figure 4 below shows and compares propeller wake vortical structures from LES (colored by pressure coefficient) to those from experiments. As can be seen in this figure LES predicts the wake vortices exceptionally well and similar to the experimental ones (Felli et al 2011).

vortex sheets begin to loose contact from their parent tip vortex. The detached helical vortex sheets then start interacting with the previously shed tip vortex. This is accompanied by short wave instabilities in the tip vortical filaments as shown in Figure 6. Ultimately the helical vortex sheets from tip vortex 4 and 5 become completely detached and then reattach to the previously shed tip vortices at position 5 and 6 respectively (Figure 5). This is then accompanied by the initiation of long wave instabilities and breakup in the tip-vortical filaments as shown in Figure 6.

Moreover, it is suggested here that the final breakup mechanisms in the far wake are different from the triggering mechanisms and thus need to be analyzed in that perspective. In this regard, (Figures 5 and 6); the mutual interaction among adjacent tip-vortex filaments begins to occur in the far wake with the distance between adjacent filaments decreasing. At the same time the magnitude of both short and long wave instabilities continues to increase in the tip vortical structures. While short wave instabilities also start to appear in the hub vortex. As the distance between adjacent vortex filaments

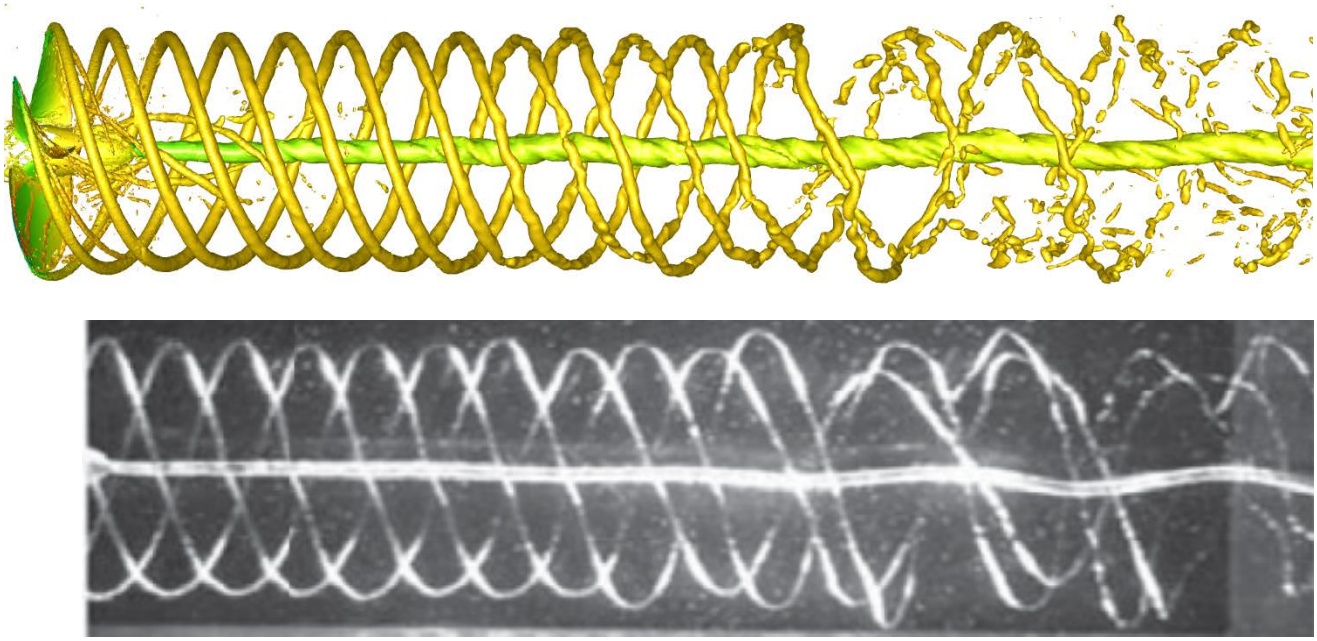

Figure 4: Comparison of wake vortical structures between LES and experiments (Felli et al 2011)

3 INSTABILITY IDENTIFICATION

The instability triggering mechanisms are primarily identified in the transition region as it is here where the propeller wake starts to undergo gradual destabilization. Various forms of instabilities have been observed along with a new phenomenon that is the helical vortex sheets mutual interaction. As shown in Figure 5, the distance between adjacent helical sheets of vortices starts to decrease especially near the stronger rectilinear hub-vortex. After this, two phenomena appear to occur simultaneously at the tip vortex position 3, as depicted in Figure 5. First, the helical vortex sheets begin to interact with the adjacent helical sheets and second, the helical approaches zero, leap-frogging of vortices begins to occur in the far wake. Leap frogging occurs in both pairs of the four filaments shed from the four blade-tips of the propeller under consideration. As the first pair mutually interacts and attracts and undergoes leap frogging, it repels the other pair undergoing the same process. This is then accompanied by the appearance of long waves in the hub-vortex which until this point in time and space had remained rectilinear. Ultimately, after undergoing a few leap-frogging cycles, the tip vortical structures breakdown completely (Figure 4). This is followed by the hub vortex breakdown (further downstream, not shown) resulting in the total collapse of these fascinating wake vortical structures behind the ship propeller.

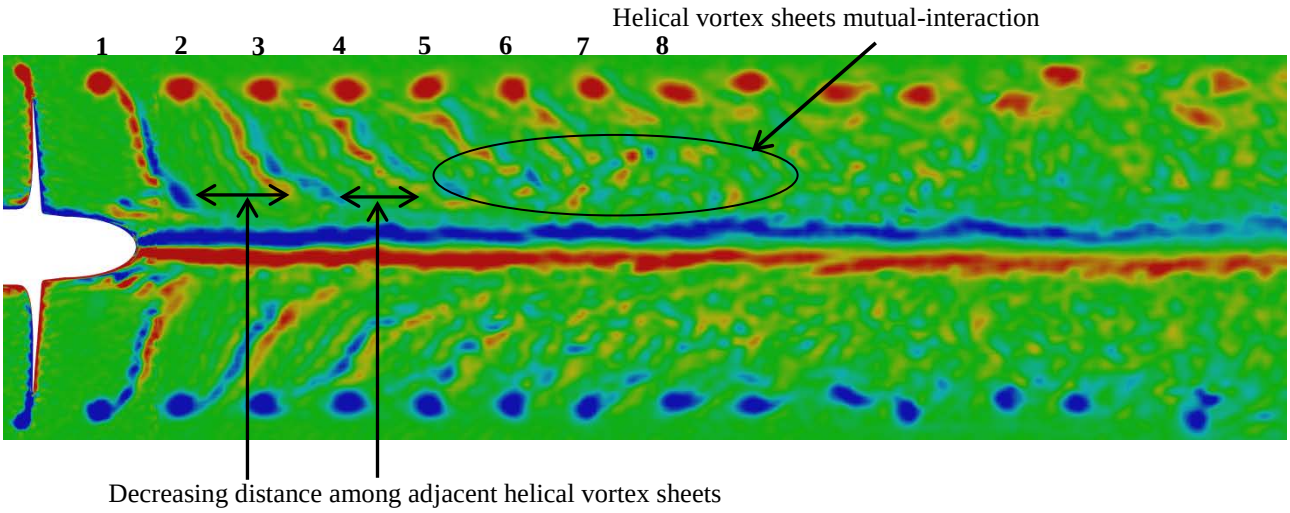

Figure 5: Out-of-plane vorticity contours on the mid-longitudinal plane

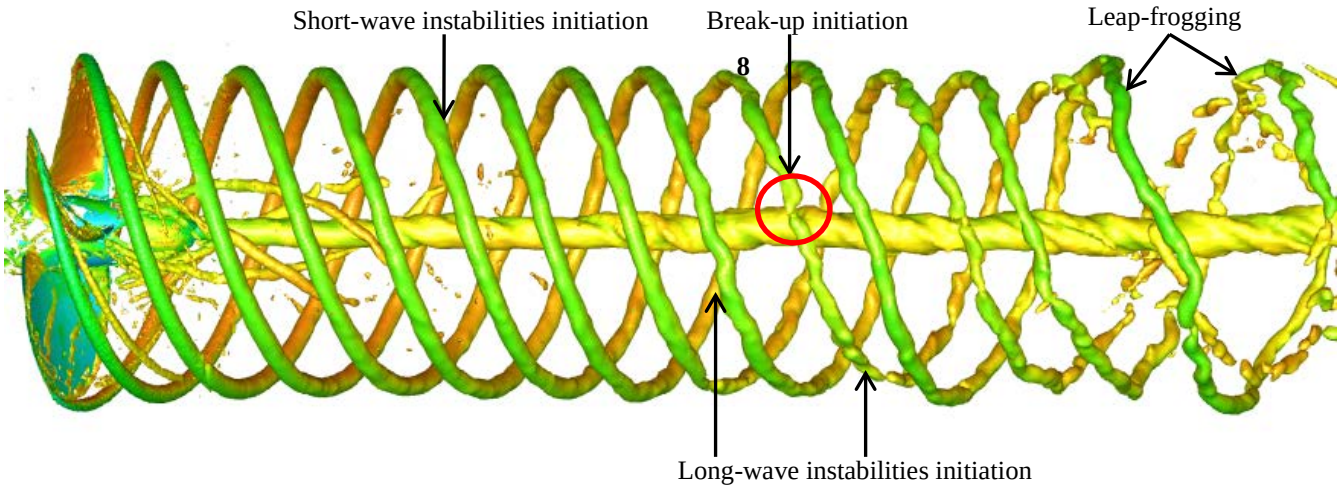

Figure 6: Instabilities in the wake vortical structures (colored by axial velocity)

4 CONCLUSIONS

An analysis of propeller wake characteristics and mechanisms leading to wake breakdown is completed for a higher range advance coefficient using LES. LES has been shown to describe the propeller wake geometry from evolution to far wake breakdown similar to that obtained from previously published experiments. Mechanisms instigating propeller wake instabilities and mechanisms responsible for ultimate wake breakdown have been separately identified. These mechanisms have been linked and appropriately correlated. A new mechanism in regard to mutual interaction among vortices in the adjacent helical vortex sheets has also been observed for which further research is currently underway for a range of advance coefficients.

REFERENCES

ANSYS (2016). ANSYS Fluent Theory Guide. ANSYS Inc.

Davidson, L. (2009). 'Large Eddy Simulations: How to evaluate resolution'. Int. J. Heat Fluid Fl. **30**(5), 1016–1025.

Gupta, B.P. & Loewy, R.G. (1974). 'Theoretical analysis of the aerodynamic stability of multiple, interdigitated helical vortices', AIAA J. **12**(10), 1381–1387.

Felli, M., Camussi, R. & Felice, F.D. (2011). 'Mechanisms of evolution of the propeller wake in the transition and far fields'. J. Fluid Mech. **682**, 5–53.

Muscari, R., Mascio, A.D. & Verzicco, R. (2013). 'Modeling of Vortex Dynamics in the Wake of a Marine Propeller'. Comput. Fluids **73**, 69–79.

Kumar, P. & Mahesh, K. (2017). 'Large eddy simulation of propeller wake instabilities'. J. Fluid Mech. **814**, 361–396.

Okulov, V.L. & Sørensen, J.N. (2007). 'Stability of helical tip vortices in a rotor far wake'. J. Fluid Mech. **576**, 1–25.

Salvatore, F., Testa, C., Ianniello, S. & Pereira, F. (2006). 'Theoretical modelling of unsteady cavitation and induced noise'. in Proceedings of the 6th International Symposium on Cavitation, Netherlands.

Shur, M. L., Spalart, P. R., Strelets, M. K. & Travin A. K. (2008). 'A hybrid RANS-LES approach with delayed-DES and wall-modelled LES capabilities'. Int. J. Heat Fluid Fl. **29**(6), 1638–1649.

Stella, A., Guj, G., Felice, F.D. & Elefante, M. (2000). 'Experimental investigation of propeller wake evolution by means of LDV and flow visualizations'. J. Ship Res. **44**(3), 155–169.

Widnall, S.E. (1972). 'The stability of a helical vortex filament'. J. Fluid Mech. **54**(4), 641–663.